Molecular Biology of the Cell
Vol. 18, 4155–4167, October 2007

Regulation of the Formin for3p by cdc42p and bud6p[D] [V]

Sophie G. Martin,*† Sergio A. Rincón,‡ Roshni Basu,* Pilar Pérez,‡ and Fred Chang*

*Department of Microbiology, College of Physicians and Surgeons, Columbia University, New York, NY 10032; and ‡Instituto de Microbiología Bioquímica, Departamento de Microbiología y Genética, Consejo Superior de Investigaciones Científicas/Universidad de Salamanca, 37007 Salamanca, Spain

Submitted February 2, 2007; Revised July 31, 2007; Accepted August 3, 2007
Monitoring Editor: Thomas Pollard

Formins are conserved actin nucleators responsible for the assembly of diverse actin structures. Many formins are controlled through an autoinhibitory mechanism involving the interaction of a C-terminal DAD sequence with an N-terminal DID sequence. Here, we show that the fission yeast formin for3p, which mediates actin cable assembly and polarized cell growth, is regulated by a similar autoinhibitory mechanism in vivo. Multiple sites govern for3p localization to cell tips. The localization and activity of for3p are inhibited by an intramolecular interaction of divergent DAD and DID-like sequences. A for3p DAD mutant expressed at endogenous levels produces more robust actin cables, which appear to have normal organization and dynamics. We identify cdc42p as the primary Rho GTPase involved in actin cable assembly and for3p regulation. Both cdc42p, which binds at the N terminus of for3p, and bud6p, which binds near the C-terminal DAD-like sequence, are needed for for3p localization and full activity, but a mutation in the for3p DAD restores for3p localization and other phenotypes of *cdc42* and *bud6* mutants. In particular, the for3p DAD mutation suppresses the bipolar growth (NETO) defect of *bud6*Δ cells. These findings suggest that cdc42p and bud6p activate for3p by relieving autoinhibition.

INTRODUCTION

Formins are key regulators of the actin cytoskeleton and form a large family conserved in all eukaryotes (Wallar and Alberts, 2003; Faix and Grosse, 2006). These proteins are necessary for the formation of numerous actin structures, including stress fibers, filopodia, cytokinetic actin rings, junctional actin structures, or actin cables. The proper regulation of formins is likely to be critical for cellular processes such as cell migration, cytokinesis, cell adhesion, and cell polarity.

A well characterized biochemical activity of formins is to nucleate and elongate linear actin filaments (Pruyne *et al*., 2002; Sagot *et al*., 2002b; Kovar *et al*., 2003; Li and Higgs, 2003; Moseley *et al*., 2004). This activity occurs through the formin-homology (FH) 2 domain, which dimerizes to form a doughnut-shaped structure containing multiple actin-binding sites in its core (Xu *et al*., 2004; Otomo *et al*., 2005b). This dimer is thought to stabilize otherwise unstable intermediates in the assembly of new actin filaments, and it binds processively to the fast-elongating barbed end of existing actin filaments (Pring *et al*., 2003; Kovar and Pollard, 2004). The adjacent FH1 domain binds profilin-actin and helps accelerate the elongation of actin filaments (Chang *et al*., 1997; Evangelista *et al*., 1997; Watanabe *et al*., 1997; Romero *et al*., 2004; Kovar *et al*., 2006). The budding yeast formin Bni1p also binds the actin monomer-binding protein Bud6p, which, similar to profilin, stimulates the activity of the FH2 domain (Moseley and Goode, 2005). In addition to their activity in actin filament nucleation and elongation, some formins have been suggested to also function in actin bundling and severing, further contributing to the remodeling of actin structures (Harris *et al*., 2004, 2006; Moseley and Goode, 2005; Harris *et al*., 2006).

The potent activity of formins needs to be carefully regulated in vivo to generate the correct actin structures at the right place and time. Autoinhibition has been proposed to be an important mechanism by which formin activity is controlled. Initially discovered in diaphanous-related formins, this mechanism relies on the interaction of a conserved C-terminal motif, named *D*iaphanous *A*utoregulatory *D*omain (DAD), with the *D*iaphanous *I*nhibitory *D*omain (DID) in the N-terminal region (Watanabe *et al*., 1999; Alberts, 2001; Li and Higgs, 2003, 2004; Wallar *et al*., 2006). Support for this model largely came from the observation that exogenous expression of truncated formin constructs, lacking either N or C terminus, or harboring a mutated DAD region, led to an overabundance of actin structures, such as filopodia or stress fibers (Watanabe *et al*., 1999; Tominaga *et al*., 2000; Koka *et al*., 2003; Schonichen *et al*., 2006; Wallar *et al*., 2006). It is not clear whether all formins use an autoinhibitory mechanism for regulation, because many formins do not contain an obvious DAD-like sequence at the primary sequence level (Higgs and Peterson, 2004).

The autoinhibition of many formins is regulated by small Rho GTPases. Different formins may be regulated by different Rho GTPases; for example, Cdc42 is thought to regulate

This article was published online ahead of print in *MBC in Press* (http://www.molbiolcell.org/cgi/doi/10.1091/mbc.E07–02–0094) on August 15, 2007.

[D] [V] The online version of this article contains supplemental material at *MBC Online* (http://www.molbiolcell.org).

† Present address: Center for Integrative Genomics, Génopode Building, University of Lausanne, 1015 Lausanne, Switzerland.

Address correspondence to: Fred Chang (fc99@columbia.edu).

Abbreviations used: DAD, Diaphanous Autoregulatory Domain; DID, Diaphanous Inhibitory Domain; FH, Formin Homology; LatA, Latrunculin A; NETO, New End Take Off.

the formins mDia2 and FRLα in mammalian cells, whereas Rho3p and Rho4p regulate Bni1p in the budding yeast (Dong *et al.*, 2003; Peng *et al.*, 2003; Seth *et al.*, 2006). Generally, specific Rho(s) bind to formins at an N-terminal G protein binding-domain partially overlapping with the DID domain. This binding activates formins by relieving the autoinhibitory interaction between the DAD and DID, because Rho competes with the DAD for DID binding (Dong *et al.*, 2003; Lammers *et al.*, 2005; Otomo *et al.*, 2005a; Rose *et al.*, 2005; Nezami *et al.*, 2006). In vitro experiments have shown that the activity of the FH1–FH2 domain is indeed inhibited by binding of the N terminus to the DAD (Li and Higgs, 2003). Binding of active Rho not only regulates the biochemical activity of formins but also may control their ability to localize to the cell cortex (Seth *et al.*, 2006). N-terminal truncations or overexpression of the DAD domain of the formin Bni1p have also been shown to suppress growth defects in *rho* mutants in budding yeast, suggesting that activation of formins is a major function of these rho proteins (Dong *et al.*, 2003). Genetic and biochemical studies are beginning to indicate the existence of additional modes of formin regulation, such as phosphorylation and through interactions with other proteins (Dong *et al.*, 2003; Li and Higgs, 2003; Matheos *et al.*, 2004; Moseley *et al.*, 2004; Martin *et al.*, 2005; Eisenmann *et al.*, 2007).

In this study, we have focused on for3p, one of the three formins in the fission yeast *Schizosaccharomyces pombe*. Fission yeast cells are rod-shaped and grow exclusively at cell tips. The formin for3p localizes to cell tips, and it is responsible for the assembly of a polarized array of actin cables (Feierbach and Chang, 2001; Nakano *et al.*, 2002). These cables are bundles of short linear actin filaments largely oriented with their barbed ends facing the cell tip (Kamasaki *et al.*, 2005). Actin cables contribute to polarized cell growth, in part, by acting as tracks for the delivery of myosin V-driven vesicles to cell tips (Schott *et al.*, 2002; Salas-Pino and Chang, unpublished observations). Analyses of for3p movements suggest that the activity and localization of for3p is highly dynamic on the time scale of seconds (Martin and Chang, 2006). At the cell tip, for3p may be active at cell tips for actin assembly for only a few seconds, before it is released onto assembling actin cables, and travels away from cell tips with the retrograde flow of actin in cables. Because only 20–30% of the total for3p protein is present at cell tips at any given time, much of for3p protein is probably inactive. How for3p is localized and regulated at the cell tip is not well understood. Based upon sequence comparisons, for3p was categorized as a DAD-less formin (Higgs and Peterson, 2004). It has been shown to bind to activated rho3p and cdc42p but not other rhos, in two-hybrid assays (Nakano *et al.*, 2002). However, the physiological significance of these interactions is not clear, especially because the function of these rhos in actin cable assembly has not yet been elucidated.

The formin for3p plays an important role in regulating the growth pattern of fission yeast cells. After cell division, cells initially grow in a monopolar manner, and then they initiate polarized growth at the second cell end in the G2 phase of the cell cycle (Martin and Chang, 2005). This transition to bipolar growth, termed *n*ew *e*nd *t*ake-*o*ff (NETO), relies on the localization of for3p to the new end. In this process, the regulation of for3p is dependent on tea1p, tea4p, and bud6p, all of which are necessary for NETO and reside in large complexes with for3p at cell tips (Verde *et al.*, 1995; Feierbach and Chang, 2001; Glynn *et al.*, 2001; Martin *et al.*, 2005). Similar to its *Saccharomyces cerevisiae* orthologue, bud6p binds to the C terminus of for3p and is required for proper for3p localization and robust actin cable assembly (Feierbach and Chang, 2001; Ozaki-Kuroda *et al.*, 2001). However, the precise functions of bud6p are unknown.

Here, we show that for3p is regulated by autoinhibition through an intramolecular interaction. We demonstrate that cdc42p is the primary Rho-GTPase for actin cable assembly and that it functions to relieve for3p autoinhibition. We further show that bud6p binds for3p at a site overlapping with the DAD, and that all *bud6*Δ phenotypes can be rescued by preventing for3p autoinhibition, suggesting that bud6p also regulates for3p autoinhibition. The proper localization of the formin depends on relief of autoinhibition and the binding of multiple sites on the formin to cortical docking factors. Finally, these studies address how regulation of for3p contributes to controlling bipolar cell growth.

MATERIALS AND METHODS

Yeast Strains, Media, and Genetic Methods

The *S. pombe* strains used in this study are listed in Supplemental Table 1. Standard methods for *S. pombe* media and genetic manipulations were used throughout. All plasmids were sequenced. Tagged strains were constructed using a polymerase chain reaction (PCR)-based approach and confirmed by analytical PCR.

The *for3DAD** and *for3*Δ*FH3* mutations were created by PCR stitching in two rounds of PCR to generate pGBD-for3(1261-1461)LLT-AAA and pREP42-EGFP-for3NΔ(353-406), respectively. All plasmids used in this study are listed in Supplemental Table 2. To generate the *for3DAD** and *for3*Δ*FH3* alleles in vivo, the genomic *for3* DAD and FH3 regions were replaced with *ura4*$^+$ in a wild-type strain, to yield strain YSM816 and YSM327, respectively. These strains were transformed with a linearized *for3DAD** or *for3*Δ*FH3* fragment. *ura4*$^-$ colonies were selected on 5-fluoroorotic acid, and integration was confirmed by PCR and sequenced.

To isolate *cdc42* mutants, we introduced random mutations into the entire region of *cdc42* by the error-prone PCR method (Cadwell and Joyce, 1992). PCR was carried out with AmpliTaq DNA polymerase (PerkinElmer-Cetus, Boston, MA) in manufacturer-supplied reaction buffer mixtures containing 1 mM dCTP/dTTP and 0.2 mM dGTP/dATP, 2.5 mM $MgCl_2$, with 100 ng/100 μl reaction mixture of purified pSK*cdc42* as a template. Oligonucleotide primers 5′-TATATACATATGCCCACCATTA AGTGTGTC-3′ and 5′-TATAGGATCCTTACAGTACCAAACACTTTGAC-3′ were designed to amplify the entire *cdc42* open reading frame (ORF) flanked by NdeI–BamHI (underlined). The collection of *cdc42* ORFs was cloned into a Bluescript plasmid, in which 500 base pairs of the *cdc42* 5′ region and 500 base pairs of the *cdc42* 3′ region had previously been cloned on either side of the kanamycin resistance gene (*KanMX*). The ORFs were cloned adjacent to the 5′ region by using the NdeI–BamHI sites. A second PCR amplification was used to generate a DNA fragment, including 5′ region-*cdc42-KanMX*-3′region, with free ends homologous to the flanking regions of *cdc42*$^+$. This fragment was used to transform an *h+ leu1-32 ura4D-18* (PPG103) strain. Transformant clones were selected in YES+G418 plates at 25°C and screened for thermosensitivity at 36.5°C. Colonies that exhibited temperature-sensitive (*ts*) growth were selected and the *cdc42* allele carried by one of them was named *cdc42-1625* and analyzed further.

To generate hemagglutinin (HA)-cdc42 and HA-cdc42-1625 strains, a genomic version of *cdc42*$^+$ or *cdc42-1625* with the HA epitope coding sequence fused at the beginning of the ORF was generated by inserting in a Bluescript plasmid 500 base pairs of the 5′ *cdc42* flanking sequences, the *HA* sequence, the *cdc42*$^+$ or *cdc42-1625* ORF, the *ura4*$^+$ gene, and 500 base pairs of the 3′ *cdc42* flanking sequence. The insert was transformed into an *h+ leu1-32 ura4D-18* (PPG103) strain, and stable transformants were selected and screened by PCR for the appropriate gene replacement

We found that *cdc42-1625 bud6* double mutants were strictly dependent on the presence of a pREP41-HA-*cdc42* plasmid for growth; although this plasmid was lost from >20% of *cdc42-1625* single mutant cells grown in nonselective media for >10 generations, it was not lost from *cdc42-1625 bud6*Δ cells, demonstrating that this double mutant is not viable.

Microscopy

Microscopy was performed using either a widefield fluorescence microscope or a spinning disk confocal microscope essentially as described previously (Martin and Chang, 2006), and images were acquired, processed, and analyzed with the OpenLab software (Improvision, Coventry, United Kingdom).

To prepare cells for live imaging of green fluorescent protein (GFP) or red fluorescent protein (RFP)-tagged proteins, strains were grown in Edinburgh minimal media supplemented with appropriate amino acids and 5 times the amount of adenine overnight at 30°C to log phase (or 25°C for *cdc42-1625* strains and corresponding wild-type controls) and observed at room temper-

ature (22–24°C), unless otherwise noted. To image live actin cables, GFP–CH domain expression was induced for 16 h in medium lacking thiamine. To image GFP-for3N, expression was induced for 14–16 h in medium lacking thiamine. For all other imaging, cells were grown in YE5S medium at 30 or 25°C, unless noted otherwise. Actin staining was performed as described using AlexaFluor 488-phalloidin (Invitrogen, Carlsbad, CA) with a fixation time of 40 min (Pelham and Chang, 2001). For actin staining of GFP-tagged strains, AlexaFluor 488-phalloidin was also used, because the GFP signal was not resistant to the fixation and staining procedure, and thus it did not interfere with imaging of the actin cytoskeleton (data not shown). We prepared 100X stock solutions of latrunculin A (LatA) (provided by Phil Cruz, University of California, Santa Cruz) in dimethyl sulfoxide.

For HA–Cdc42p localization, cells were fixed with methanol-free 16% formaldehyde (Polysciences, Warrington, PA) for 40 min as described (Hagan and Hyams, 1988). Cells were incubated for 16 h at 4°C with a 1:200 dilution of anti-HA antibody in PEMBAL. Then, 3 × 1 h washes with PEMBAL [100 mM piperazine-N, N′-bis(2-ethanesulfonic acid) pH 6.9, 1 mM EGTA, 1 mM $MgSO_4$, 1% bovine serum albumin, 100 mM L-lysine hydrochloride, 0.1% NaN_3] at room temperature were performed. Cells were incubated for 2 h at room temperature with a 1:1000 dilution of anti-mouse AlexaFluor 594-conjugated antibody; Invitrogen). Then, we preformed 3 × 1 h washes with PEMBAL at room temperature before cells were analyzed under the microscope.

Data Analysis

For3p movements were analyzed with kymographs, which were constructed using the "Volume Slicing" tool of the OpenLab software, as described previously (Martin and Chang, 2006). Fluorescence activation after photobleaching (FRAP) analysis was performed as described previously (Martin and Chang, 2006).

Quantification of the fluorescence intensity of actin cables was performed using ImageJ software (National Institutes of Health, Bethesda, MD). We drew a line roughly perpendicular to the long axis of the cell across actin cables in the middle third of the cell (making sure the line did not cross actin patches), and we measured the peaks of the fluorescence profile along this line with the "plot profile" tool. From each maximum value, we subtracted the background fluorescence (level of the fluorescence profile outside the cell). Note that the fluorescence value is arbitrary and varies from one experiment to the other depending on imaging conditions, but that under identical staining and imaging conditions, in five of five experiments *for3DAD** cells show stronger actin cables than wild-type cells. Length and width of cells was measured on calcofluor-stained septated cells in the middle of the short and long axis, respectively.

Two-Hybrid Analysis, In Vitro Binding Assays, and Western Blotting

Two-hybrid interactions were tested on medium lacking histidine in strain AH109 (Clontech, Mountain View, CA). Maltose binding protein (MBP) and MBP-for3N(1-702) were expressed in *E. coli*, affinity purified on an amylose resin (Clontech), and stored at 4°C on the resin in the presence of sodium azide. 6His-tagged for3C(630-1461) and for3CDAD*(630-1461) were expressed in *E. coli*, purified on nickel columns, eluted in 250 mM imidazole, and stored at −80°C. In vitro binding assays were performed in microbio-spin columns (Bio-Rad, Hercules, CA) by adding equivalent amounts of His-tagged protein diluted eight times in B buffer (20 mM Tris, pH 8.0, 20 mM KCl, 130 mM NaCl, 1 mM $MgCl_2$, and 2 mM EDTA) to MBP fusion-coupled amylose resin and incubating for 2 h at 4°C. The resin was subsequently washed three times with B buffer and one time with B buffer + 0.05% NP-40 and two times with B buffer. MBP-fusions and associated proteins were eluted in 50 μl of 10 mM maltose. After addition of sample buffer, samples were analyzed by SDS-polyacrylamide gel electrophoresis, Coomassie staining, and Western blotting.

Antibodies used were as follows: monoclonal mouse anti-HA (HA.11, Covance; or 12CA5, Roche Diagnostics, Indianapolis, IN), monoclonal mouse anti-polyhistine (HIS-1; Sigma-Aldrich, St. Louis, MO), monoclonal mouse anti-GFP (clones 7.1 and 13.1; Roche Diagnostics), anti-actin antibody (MP Biomedicals, Irvine, CA), and monoclonal anti-α-tubulin (TAT).

RESULTS

Cdc42p Is Necessary for Cell Morphology, Actin Cables, and for3p Localization

Small Rho GTPases bind and regulate formins in many organisms. In the fission yeast, activated alleles of rho3p and cdc42p have been shown to bind the N-terminal region of for3p (Nakano *et al*., 2002); however the functional significance of these interactions has not been explored. For3p localization and actin cable organization seemed normal in *rho3*Δ cells (data not shown), suggesting that rho3p may not be the major regulator of for3p. Therefore, we focused our attention to cdc42p.

cdc42$^+$ is an essential gene (Miller and Johnson, 1994), and so we generated point mutant alleles (see *Materials and Methods*). In this study, we characterized one of these alleles, *cdc42-1625*. Strains bearing this allele were temperature sensitive for growth at 36°C (Figure 1, A and B). This growth defect was rescued by wild-type *cdc42*$^+$ and the constitutively active allele *cdc42G12V* expressed from plasmids, but not by the inactive allele *cdc42T17N* (Figure 1B), indicating that *cdc42-1625* is a hypomorphic allele.

DNA sequencing of this allele revealed a single mutation that substitutes the alanine residue at position 159 for valine. This residue, close to the C terminus, is conserved in Cdc42 from different species, including mammals, and maps to one of the four Cdc42 domains implicated in GTP binding and hydrolysis (Johnson, 1999). Immunoblots showed that the cdc42p-1625 mutant protein was expressed but exhibited faster mobility and decreased levels at 36°C compared with wild-type cdc42p (Figure 1C). In contrast, wild-type cdc42p levels were higher at 36°C than at 25°C. The cdc42p-1625 protein was still properly localized to growing cell tips and septa, suggesting that this mutation does not affect membrane association (Figure 1D). *cdc42-1625* mutant phenotypes described below were apparent at both 25 and 36°C, suggesting that function was lost even at 25°C. The growth defect at 36°C may be due to a higher requirement of cdc42p at elevated temperatures. Subsequent experiments described in this article were thus conducted at 25°C, except where noted.

We next tested the effect of cdc42p on cell morphology and actin cable formation. *cdc42-1625* cells were misshapen and sometimes displayed misplaced septa (Figure 1E). Cells showed more pronounced morphological defects and increased cell lysis at 36°C (Figure 1E). Significantly, *cdc42-1625* cells had very few short, weakly staining actin cables at both 25 and 36°C, as shown by AlexaFluor-phalloidin staining (Figure 1G). Actin patches were depolarized from cell tips in >90% of cells (n > 100), a possible consequence of the cable defect. To probe the function of actin cables, we also examined the distribution of a barbed end-directed type V myosin, which is normally targeted to cell tips by moving on actin cables (Motegi *et al*., 2001). Using a myo52p-tomato fusion, we found that myo52p dots failed to accumulate at cell tips in >90% of *cdc42-1625* cells (n = 200; Figure 1H), consistent with defects in actin cable organization. Expression of *cdc42*$^+$ in *cdc42-1625* cells rescued the morphological and actin cable defects (Figure 1F).

To examine for3p distribution, we used a for3p fusion construct tagged with three tandem copies of GFP; this fusion is expressed from the chromosomal *for3* locus from the endogenous promoter and is functional (Martin and Chang, 2006). In *cdc42-1625* strains, for3p-3GFP failed to accumulate at cell tips (Figure 6I). Thus, similar to what has been seen with many diaphanous-related formins (Watanabe *et al*., 1997; Gasman *et al*., 2003; Gasteier *et al*., 2003; Peng *et al*., 2003; Seth *et al*., 2006), cdc42p is required for the efficient localization of full-length for3p to cell tips. Thus, cdc42p is the primary Rho protein in fission yeast responsible for regulation of actin cable assembly and formin for3p localization.

For3p Contains Three Localization Domains

To study the mechanisms responsible for for3p regulation, we next used a mutational approach to define sites on for3p that affect its localization and activity. We and others previously showed that the N terminus of for3p (amino acids [aa] 1-702; for3N) is sufficient to localize to cell tips (Nakano *et al*.,

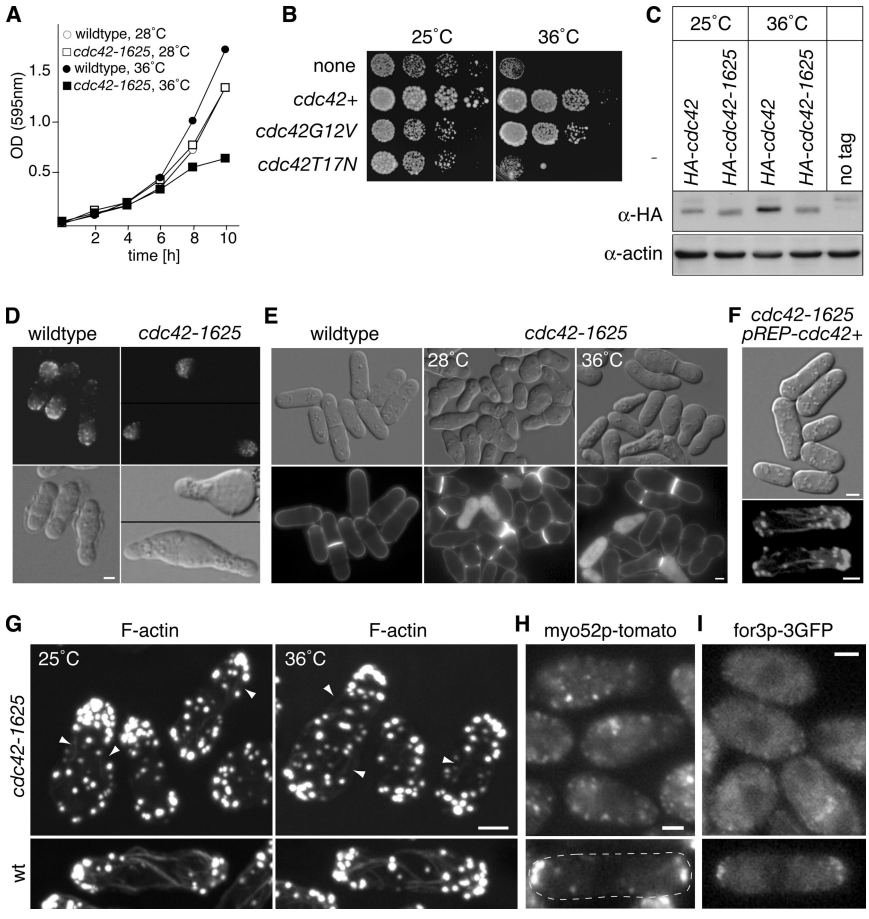

Figure 1. Cdc42p is necessary for cell morphology, actin cable organization and for3p localization. (A) Growth curve of wild-type and *cdc42-1625* cells incubated at 28 and 36°C. (B) Rescue of the temperature-sensitive growth defect of *cdc42-1625* by different *cdc42* alleles. *cdc42-1625* cells were transformed with the expression plasmid pREP41-HA carrying either no insert, wild-type *cdc42*$^{+}$, constitutively active *cdc42G12V*, or dominant-negative *cdc42T17N* alleles and grown on Edinburgh minimal media plates for 2 d at 25 and 36°C. (C) Immunoblot of HA-cdc42p and HA-cdc42p-1625 expressed from the endogenous promoter. Twenty-five micrograms of total yeast extracts from exponential cultures at 25 and 36°C were loaded in each lane. Levels were monitored with the anti-actin antibody. Although wild-type cdc42p shows increased levels at 36°C, this increase failed to happen in the *cdc42-1625* mutant. (D) Immunofluorescence of HA-cdc42p and HA-cdc42p-1625 with anti-HA antibody. Both wild-type and mutant cdc42p localize to growing cell tips. Differential interference contrast (DIC) of the permeabilized cells is shown at the bottom. (E) Morphology of wild-type and *cdc42-1625* cells grown to log phase at 28 and 36°C for 5 h. DIC and calcofluor-staining images are shown. (F) Rescue of cell morphology (DIC; top) and actin cables (AlexaFluor-phalloidin; bottom) by wild-type *cdc42*$^{+}$ in *cdc42-1625* cells at 36°C. (G) Projection images of spinning disk confocal stacks of AlexaFluor 488-phalloidin–stained *cdc42-1625* (top) and wild-type (bottom) cells grown at 25°C (left) or 36°C for 1 h (right). Note that actin cables are extremely weak, but they were still present in *cdc42-1625* cells (arrowheads). (H) Single focal plane widefield fluorescence images of myo52p-tomato in *cdc42-1625* (top) and wild-type (bottom) cells grown at 25°C. (I) Single focal plane widefield fluorescence images of for3p-3GFP in *cdc42-1625* (top) and wild-type (bottom) cells grown at 25°C. Note that for3p largely fails to localize to cell tips in the mutant cells. All bars, 2 μm.

2002; Martin *et al.*, 2005) (Figure 2B). This N-terminal region also contains a Rho-binding site (Nakano *et al.*, 2002). Residues in this region can be aligned, albeit poorly, to the DID and dimerization domains of mDia (Supplemental Figure 1). The predicted FH3 region (aa 306–507, as defined by SMART) corresponds to the C-terminal part of this DID and dimerization-like domains.

Further truncation analyses showed that the DID and dimerization-like domains (aa 137–515) were sufficient for cell tip localization (Figure 2B). In contrast, a 54 amino acid in-frame deletion within the DID (for3NΔ353-406) abrogated cortical association of the for3N fragment (Figure 2B). Because this region contains a potential dimerization domain (Otomo *et al.*, 2005a; Rose *et al.*, 2005), we verified that for3N was not localizing to the cortex just by binding to the endogenous full-length for3p: GFP-for3N also localized normally in a *for3*Δ mutant (data not shown). Thus, the N-terminal portion of for3p contains a localization domain in a region of for3p that overlaps with the DID.

Additional sites in the C-terminal portion of the protein also seem to contribute to for3p localization. We expressed the C-terminal half of for3p (aa 630-1461; for3C), including the FH1 and FH2 domains, as a GFP fusion from a plasmid. GFP-for3C localized to two distinct cellular structures: actin cables and cell tips (Figure 2C). Both localizations were present even when the fragment was expressed in *for3*Δ mutants (data not shown). The cable staining was distributed evenly throughout the cable, in a different pattern from the discrete dots seen with full-length protein. GFP-for3C also localized to actin rings, but not actin patches. This cable localization was mediated by actin binding in the FH2 region, because a point mutation in the actin-binding interface within the FH2 domain (I930A) abolished cable localization but not the cell tip localization of for3C (Figure 2C). The cell tip distribution was clearer with this mutant, or when actin structures were disrupted with LatA (a drug that sequesters actin monomers) (Figure 2C). Together, these results using for3p fragments reveal three distinct localization domains: two cortical targeting regions that localize it to the cortex and the central FH2 domain that mediates actin cable association.

For3p Exhibits an Intramolecular Interaction Mediated by a DAD-like Domain

In diaphanous-like formins, an intramolecular DID–DAD interaction controls formin activity. We asked whether a similar mode of regulation operates in for3p. We found that for3p N- and C-terminal halves interact with each other, by using in a two-hybrid assay and also with in vitro binding assays with purified protein fragments (Figure 3). Although initial sequence searches did not reveal obvious homology to other DAD sequences (Higgs and Peterson, 2004), mapping the interaction region in the C terminus defined a 25-amino acid region necessary for binding to the N termi-

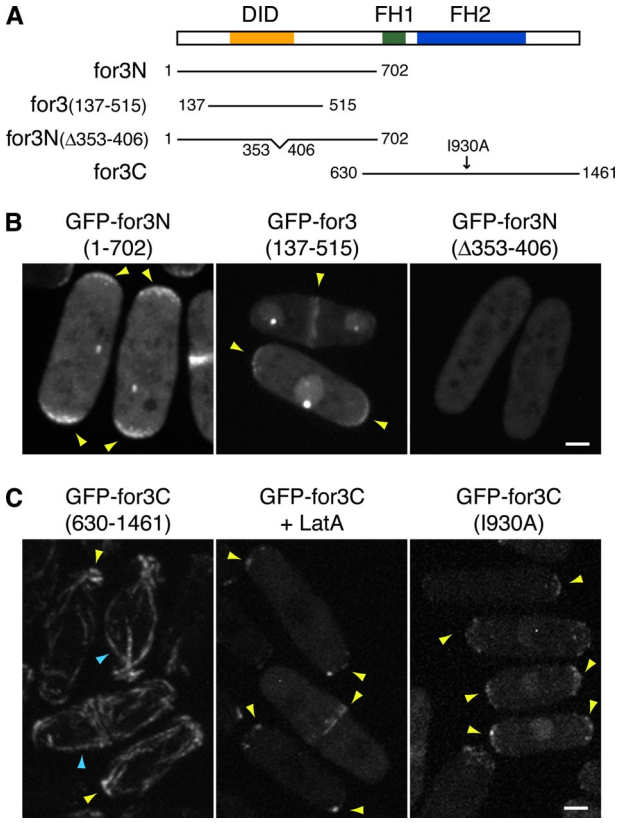

Figure 2. For3p contains three independent localization domains. (A) Scheme of for3p fragments that were fused to GFP to assay localization. All constructs were expressed from a plasmid under control of the medial-strength *nmt1* promoter. (B) Projection images of spinning disk confocal stacks of GFP-for3N (left), GFP-for3(137-515) (middle), and GFP-for3NΔ(353-406) (right). Yellow arrowheads indicate cell tips and septum localization. GFP-for3N is also detected at the spindle pole body. (C) Projection images of spinning disk confocal stacks of GFP-for3C (left), GFP-for3C treated with 200 μM LatA (middle), and GFP-for3C-I930A (right). Blue arrowhead shows actin cable localization. Yellow arrowheads indicate cell tips and septum localization.

nus of for3p (Figure 3A). This "DAD-like" region did not have strong homology with canonical DAD domains, but it did contain two leucines and a few basic residues that could be aligned with other DAD domains (Figure 3B). To test whether this putative DAD-like domain was responsible for this interaction, we mutated these residues to alanines—(1396)LLT(1398), or R(1409), K(1411), and K(1413). In the two-hybrid assay, these mutations abolished binding to a fragment of the for3p N terminus. These mutations specifically affected binding to the N terminus of for3p, because they did not affect binding to bud6p or localization of for3C to cell tips (Figure 3, A–C; data not shown) (Feierbach *et al.*, 2004).

Phenotype of a for3DAD Mutant*

We next tested the function of this intramolecular interaction in vivo. Because previous studies on formin autoinhibition commonly carry caveats of overexpression, we expressed a for3p DAD mutant protein at endogenous levels. The wild-type *for3*$^+$ gene on the chromosome was replaced with a *for3DAD** mutation that carries one of the DAD mutations described above [(1396)LLT(1398) to alanines mutation] in the full-length *for3* gene. This *for3* allele was thus expressed from the endogenous *for3* promoter as the sole *for3* gene in the cell. Western blot analysis confirmed that for3pDAD* is expressed at the same level as wild-type for3p (Figure 4A).

This for3pDAD* mutant protein was localized properly. To assess the localization of for3pDAD*, we tagged it with two tandem copies of GFP. For3pDAD*-2GFP localized efficiently to cell tips and septa. Time lapse showed dynamic behavior indistinguishable from wild-type for3p. Small dots of for3pDAD*-2GFP displayed linear movements away from cell tips at the same rate as wild-type for3p-3GFP (rate of 0.29 ± 0.09 μm/s, n = 63 vs. 0.30 ± 0.12 μm/s for wild-type under the same conditions, n = 42), and FRAP analysis showed turnover rates at cell tips similar to wild-type for3p ($t_{1/2}$ = 10–12 s) (Figure 4B and Supplemental Movies 1 and 2). The only slight difference we noticed was that for3pDAD*-2GFP seemed to display a somewhat tighter distribution at cell tips than wild-type for3p-3GFP (Figure 4C). Thus, the dynamic behavior of for3p is not primarily controlled by DAD-dependent regulation. In addition, because the rate of for3p dot movement corresponds to that of actin cable assembly (Martin and Chang, 2006), this suggested that the rate of actin polymerization was also not affected by the DAD mutation.

*for3DAD** cells had consistently more robust actin cables than wild-type, as revealed by phalloidin staining (Figure 4D). These cables were arranged in a longitudinal manner as in wild type, but quantification of their fluorescence intensity showed that they were more brightly stained than their wild-type counterpart. This result was confirmed and quantified in five independent experiments comparing side-by-side staining of nontagged and GFP-tagged *for3* and *for3DAD** cells. One representative quantification is shown in Figure 4E. We probed the dynamic properties of these cables by inhibiting actin polymerization with LatA. The cables in *for3DAD** cells depolymerized in the same time period as those in wild-type cells, suggesting that the increased amounts of actin polymer in these cables was not due to overstabilization of actin filaments (data not shown). Thus, these cells may have more actin filaments in the cables; this result may be explained by the slightly increased amounts of *for3DAD** at cell tips.

The DAD* mutation had no noticeable effect on the viability and growth of cells. *for3DAD** cells were also morphologically normal, retaining their characteristic rod shape and growth patterns (Figure 8D). However, we noticed that *for3DAD** cells were slightly, but reproducibly, longer than wild-type cells, suggesting a very modest hyperpolarization (14.48 ± 0.89 μm in wild-type vs. 14.99 ± 0.94 μm in *for3DAD** mutant cells; Student's *t* test, $p < 0.00001$; n = 140).

In summary, these data suggest that interaction between the N and C termini of for3p does have an inhibitory effect on actin cable assembly in vivo. However, this DAD-dependent autoinhibition has only a relatively mild effect, and it is not responsible for many parameters involved in actin cable assembly, such as the rate of actin filament assembly, actin stabilization, or formin release from the cortex.

Function of the DID Domain

We also tested the function of the N-terminal DID domain. Because of the poor conservation of the region with the DID domains of other formins (Supplemental Figure 1), we were unable to identify specific residues that might mediate cdc42p or DAD binding. Thus, we generated a small in-frame deletion in the region [*for3Δ(353-406)*; Figure 5A]. This mutation was introduced into the context of the full-length *for3*$^+$ gene and expressed at the endogenous locus as sole *for3* copy. Based upon our truncation analysis described

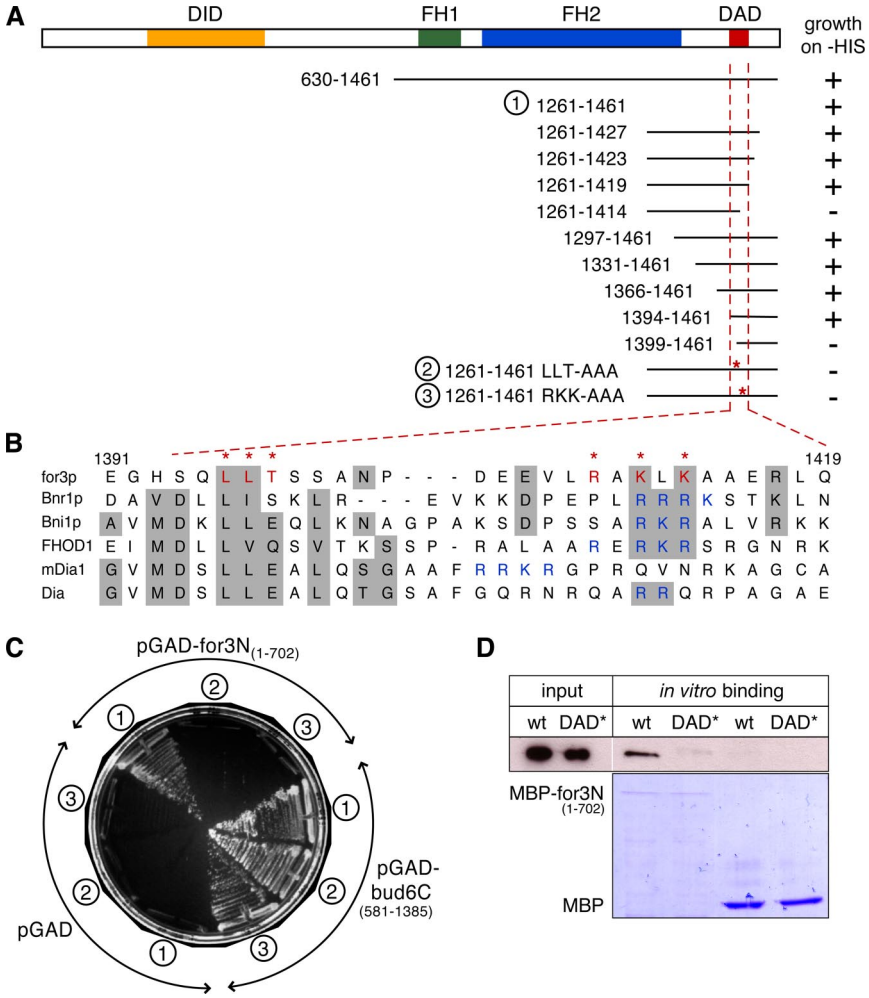

Figure 3. Identification of a DAD-like region in for3p necessary for interaction with the N terminus. (A) Mapping of the DAD domain by two-hybrid assay. Interaction of C-terminal for3p fragments cloned in the pGBD vector with pGAD-for3N(1-702) was assayed by growth on −His plates. (B) Sequence alignment of for3p DAD with defined DAD domains from *S. cerevisiae*, *Drosophila*, and mouse formins. Stretches of basic residues are shown in blue. Mutation of the residues indicated in red to alanines abolished interaction with for3p N terminus. (C) Two-hybrid assay on SC-His plate of pGAD-for3N(1-702), pGAD-bud6C(581-1385) and empty pGAD with wild-type, LLT-AAA, and RKK-AAA pGBD-for3C(1261-1461). Numbers refer to constructs indicated in A. Mutations in the DAD region specifically abolish interaction with for3N but not with bud6C. (D) 6His-for3C binds directly and specifically to MBP-for3N. Binding of bacterially expressed proteins was assayed by affinity column. 6His-for3C (aa 630-1461) binds to MBP-for3N(1-702), but not MBP alone. This interaction is compromised by the LLT-AAA mutation (DAD*). 6His-tagged protein fragments were detected by Western blotting with an anti-6His antibody. Coomassie staining of MBP-fusions indicates equal loading.

above, we predicted that this allele may be defective in aspects of cell tip localization, autoinhibition, and interaction with cdc42p.

for3Δ(353-406) cells had a more severe phenotype than the DAD* mutant. The cells were aberrantly shaped, displaying round, lemon or pear shapes, similar to *for3Δ* cells (Figure 5B). *for3Δ(353-406)* cells displayed an impressive network of actin cables, which were often disorganized or radiating from a focal point away from the cell tip (Figure 5C). Live imaging of actin cables confirmed these results and showed how cables were dynamic and often looped and organized transversally in the cell (Supplemental Movies 3 and 4). Actin patches were delocalized from cell tips in 73% of cells (n = 104). In *for3Δ(353-406)* cells, myo52p dots failed to accumulate to cell tips, but they still moved in linear paths in the cell, suggesting that the organization of actin cables was disrupted. (Figure 5D and Supplemental Movie 5). Thus, the DID domain is required for the correct organization of actin cables and for proper cell polarization.

We examined the localization of for3pΔ(353-406) by tagging it with two GFPs. For3pΔ(353-406) failed to localize efficiently to cell tips, but it still formed motile dots that moved in a linear manner in the cell (Figure 5E; data not shown). Curiously, treatment with LatA led to accumulation of this protein to cell tips. This effect suggested that in the absence of LatA, the mutant for3p may be preferentially bound to actin cables; however, after the actin cables are depolymerized in LatA treatment, for3p may be targeted to cell tips through the C-terminal cortical localization domain (Figure 5F), similar to what was seen in the for3C fragment.

Cdc42p Regulates for3p Localization by Relief of Autoinhibition

We next tested how cdc42p may affect for3p localization and/or activity. As shown above, for3p-3GFP largely failed to accumulate at cell tips in *cdc42-1625* strains. We considered two ways by which cdc42p could affect for3p localization: first, cdc42p binding at the N terminus could directly tether for3p to cell tips; second, cdc42p may be needed to alter the conformation of for3p by antagonizing for3p autoinhibition (Seth *et al*., 2006).

If cdc42p primarily regulates for3p autoinhibition, we predicted that the DAD* mutation would bypass the need for cdc42p-mediated activation. Consistent with this model, we found that for3pDAD*-2GFP efficiently localized to cell tips in *cdc42-1625* cells (Figure 6A). Thus, the localization defect seen in *cdc42* mutants is not due to loss of a cortical docking site, but rather to an inability to activate for3p.

for3DAD-2GFP* also restored a more cylindrical cell morphology to the *cdc42* mutants, making them longer and thinner (Figure 6B). Cell length and width were 14.23 ± 1.08 and 4.85 ± 0.44 μm in *cdc42-1625 for3DAD*-2GFP* (n = 70) compared with 12.88 ± 1.07 and 5.53 ± 0.54 μm in *cdc42-1625 for3-3GFP* (n = 97), respectively (Student's *t*-test, p <

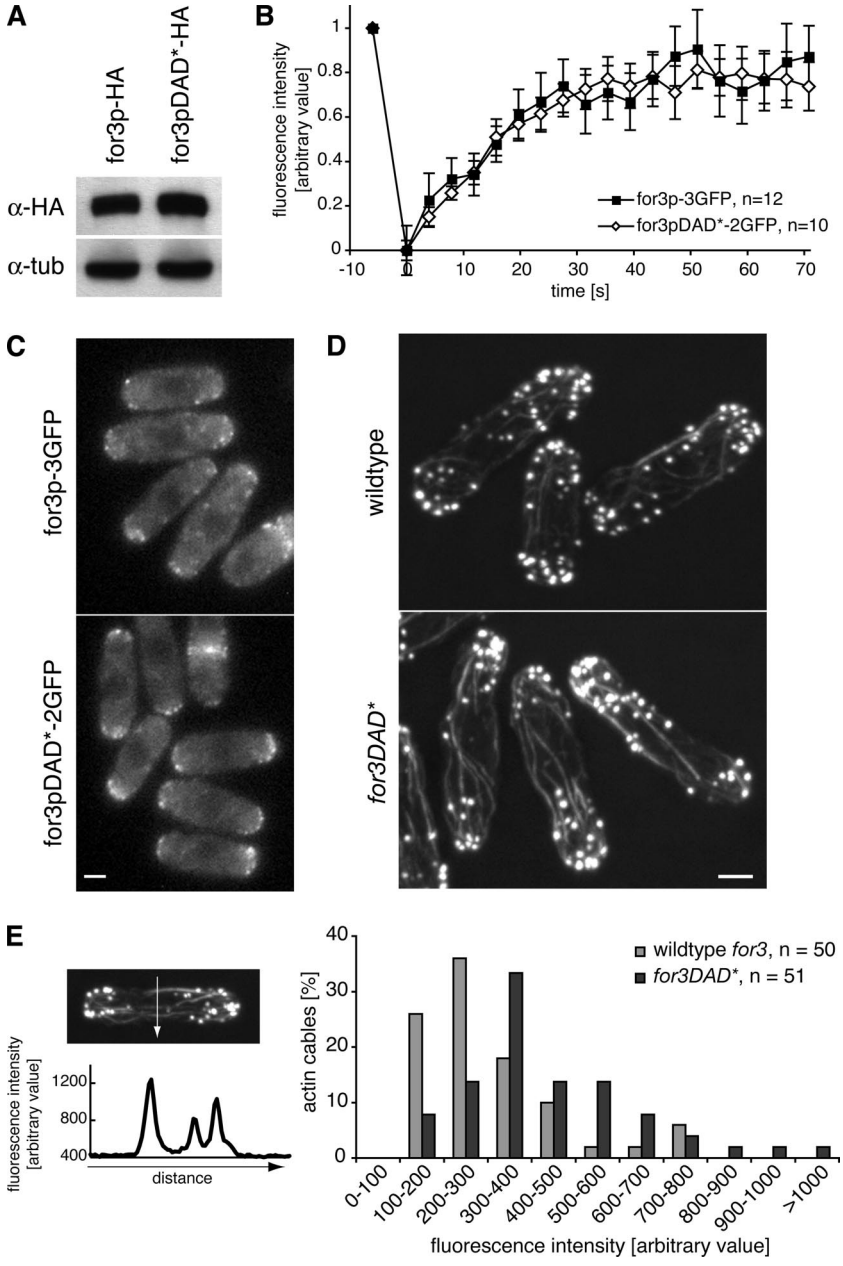

Figure 4. Phenotype of the *for3DAD** mutant. (A) Immnunoblot of for3p-HA and for3pDAD*-HA expressed from the endogenous promoter. Twelve micrograms of total yeast extract were loaded in each lane. Levels were monitored with the TAT anti-α-tubulin antibody. (B) FRAP analysis of for3p-3GFP and for3pDAD*-2GFP. Using a laser scanning microscope, the entire cell tip of cells expressing either for3p-3GFP or for3pDAD*-2GFP from the endogenous promoter was photobleached and imaged every 4 s thereafter to monitor fluorescence recovery. Each trace represents the average value for the indicated number of experiments. Error bars represent the SE. (C) Single focal plane widefield fluorescence images of for3p-3GFP and for3pDAD*-2GFP expressed from the endogenous promoter. Note that for3pDAD* localizes to cell tips, if not even more tightly than wild type for3p. (D) Projection images of spinning disk confocal stacks of AlexaFluor 488-phalloidin stained wild-type (top) and *for3DAD** (bottom) cells. Note that actin cables in the *for3DAD** mutant stain more brightly than in wild-type cells. (E) Quantification of the fluorescence intensity of actin cables in wild-type and *for3DAD** cells. We measured the peaks of the fluorescence profile along a line drawn across actin cables and subtracted background value. A histogram of these values is shown. Note that the fluorescence value is arbitrary and varies from one experiment to the other, but that under identical staining and imaging conditions, *for3DAD** cells always show stronger actin cable staining than wild-type cells.

1×10^{-13}). The localization of markers for cell polarity such as actin patches and type V myosin were also improved by the *for3DAD** mutation: myo52p-tomato dots and actin patches accumulated at the cell tip in 44 and 37% of cells, respectively (compared with <10% of *cdc42-1625* cells, n >150). However, this *for3* allele suppressed only some the defects associated with the *cdc42-1625* mutant. In particular, actin cable staining was not significantly restored (Figure 6C). This suggested that cdc42p has other effectors involved in actin cable assembly or stability.

The for3 DAD Mutation Suppresses a bud6 Mutant

Another potential for3p activator is bud6p. In both budding and fission yeasts, bud6p directly binds the C terminus of formins (Bni1p and for3p, respectively), and it is necessary for their efficient cortical localization and for efficient actin cable assembly (Ozaki-Kuroda *et al*., 2001; Feierbach *et al*., 2004; Moseley *et al*., 2004). For3p–3GFP localization to cell tips was partly compromised in *bud6*Δ cells, similar to what was shown previously. This localization defect was due to defects in cortical association and not to excessive actin cable binding, because it was not improved by LatA treatment (Figure 7B).

We defined the minimal bud6p binding site (BBS) of for3p by using the two-hybrid system (Figure 7A). Interestingly, we found that the minimal BBS overlaps significantly with the DAD in for3p. The *S. cerevisiae* BBS on Bni1p has also been mapped to a site adjacent to the DAD (Moseley *et al*., 2004). However, key amino acids mediating *S. cerevisiae* Bud6p binding are not conserved in the *S. pombe* BBS, suggesting that this site is not well conserved, at least on the level of primary sequence. We note that residues that affect DAD activity were separable from those mediating bud6p association, because the specific *for3DAD** mutation, which disrupted intramolecular binding, did not affect bud6p binding (Figure 3C).

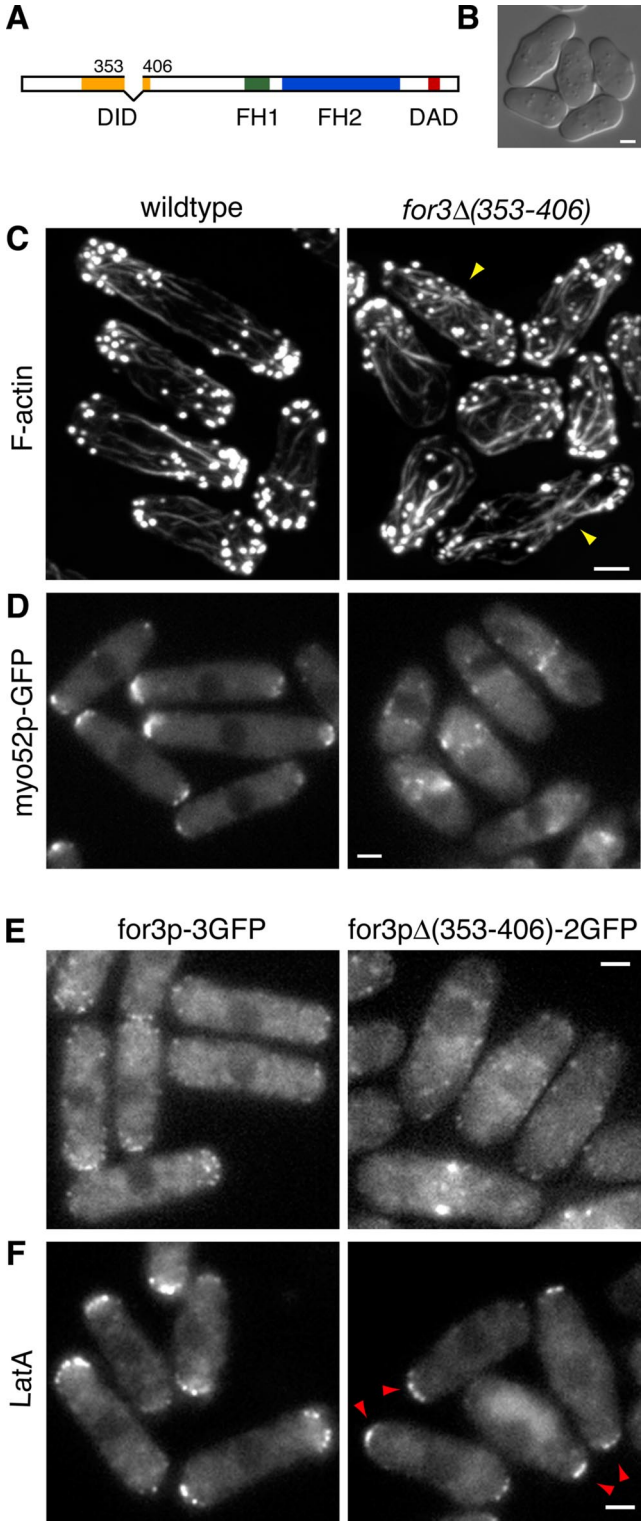

Figure 5. Deletion within the for3p DID leads to disorganized actin cables. (A) Scheme of the Δ353-406 deletion within full-length for3p. (B) DIC image of *for3Δ353-406-myc* cells. (C) Projection images of spinning disk confocal stacks of AlexaFluor 488-phalloidin–stained wild-type and *for3Δ(353-406)-myc* cells. Note the disorganized appearance of actin cables in *for3Δ(353-406)-myc* cells. Yellow arrowheads indicate locations from which some actin cables seem to radiate. (D) Single focal plane widefield fluorescence images of myo52p-GFP in wild-type (left) and *for3Δ(353-406)-myc* (right) cells. (E) Single focal plane widefield fluorescence images of for3p-3GFP (left) and for3pΔ(353-406)-2GFP (right). (F) Single focal plane widefield fluorescence images of for3p-3GFP (left) and for3pΔ(353-406)-2GFP (right) in cells treated with 200 μM LatA. Red arrowheads highlight cell tip localization of for3pΔ(353-406)-2GFP.

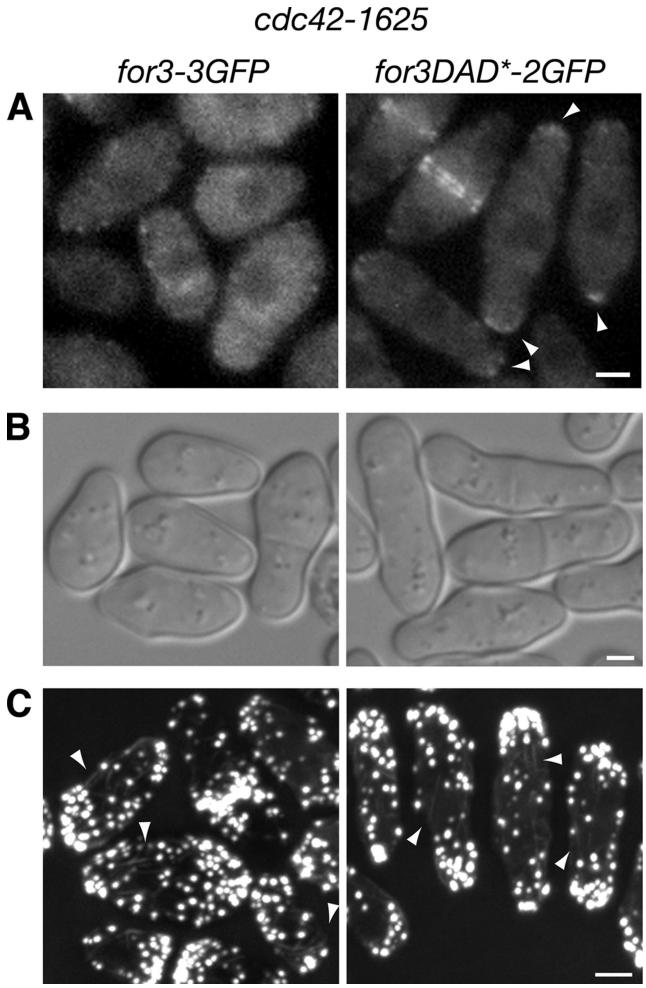

Figure 6. Cdc42p relieves for3p autoinhibition to regulate its localization. (A) Single focal plane widefield fluorescent image of for3p-3GFP (left) and for3pDAD*-2GFP (right) in *cdc42-1625* cells. Note that the DAD* mutation is sufficient to restore for3p localization to cell tips in *cdc42-1625* mutant cells (arrowheads). (B) DIC images of *for3-3GFP cdc42-1625* (left) and *for3DAD*-2GFP cdc42-1625* (right) cells. The DAD* mutation improves the morphology of *cdc42-1625* mutant cells. (C) Projection images of spinning disk confocal stacks of AlexaFluor 488-phalloidin–stained *for3-3GFP cdc42-1625* (left) and *for3DAD*-2GFP cdc42-1625* (right) cells. Arrowheads point at weak actin cables. Note that the DAD* mutation fails to restore wild-type actin cables in *cdc42-1625* mutant cells.

Bud6p binding in the vicinity of the DAD raised the question of whether bud6p may affect autoinhibition. As with *cdc42*, we found, importantly, that the DAD* mutation restored for3p localization to cell tips in *bud6*Δ cells (Figure 7C). Thus, autoinhibition, not a lack of a cortical tether, may prevent full-length for3p from localizing properly in *bud6*Δ mutants.

for3 DAD Rescues Actin Cable Assembly and Bipolar Growth Defects in bud6Δ Cells*

The *for3DAD** mutation also rescued other phenotypes associated with *bud6*Δ cells. Actin cables are generally less

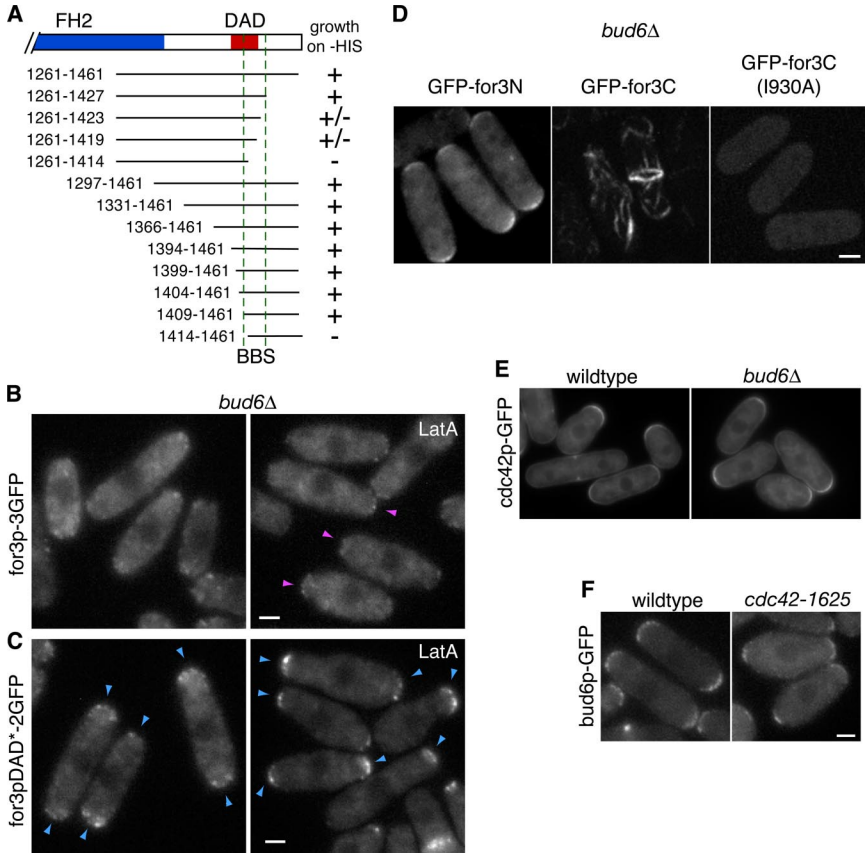

Figure 7. Bud6p targets for3p to cell tips through both anchoring and relief of autoinhibition. (A) Mapping of the BBS in for3p by two-hybrid analysis. Interaction of C-terminal for3p fragments cloned in the pGBD vector with pGAD-bud6C(581-1385) was assayed by growth on −His plates. Note how the minimum interaction domain overlaps with the DAD region. (B) Single focal plane widefield fluorescent images of for3p-3GFP in *bud6*Δ cells. Cells on the right were treated with 200 μM LatA. (C) Single focal plane widefield fluorescent images of for3pDAD*-2GFP *bud6*Δ cells. Cells on the right were treated with 200 μM LatA. Note that the DAD* mutation is sufficient to restore efficient for3p localization to cell tips in *bud6*Δ mutant cells (blue arrowheads). (D) Projection images of spinning disk confocal stacks of GFP-for3N (left) and GFP-for3C (middle), and GFP-for3C-I930A (right) expressed from the medial-strength *nmt1* promoter in *bud6*Δ mutant cells. GFP-for3C fails to localize to cell tips. (E) Single focal plane widefield fluorescent images of cdc42p-GFP in wild-type and *bud6*Δ cells. (F) Single focal plane widefield fluorescent images of bud6p-GFP in wild-type and *cdc42-1625* cells.

robust in *bud6*Δ cells (Feierbach *et al*., 2004). The *for3DAD** mutation was sufficient to restore actin cables in these cells, as measured by fluorescence intensity of AlexaFluor-phalloidin staining (Figure 8, A and B).

Bud6p has also been shown to be required for the efficient initiation of a second site of polarized growth at NETO (Glynn *et al*., 2001). It is not known whether this function depends on for3p or represents an independent activity of bud6p. Remarkably, the *for3DAD** allele was sufficient to restore bipolar growth in *bud6*Δ cells: whereas only ~40% of *bud6*Δ cells initiate a second site of growth, >70% of *bud6*Δ *for3DAD** cells undergo NETO and grow in a bipolar manner (Figure 8, C and D). Similar results were obtained using *for3*$^{+}$ and *for3DAD** alleles tagged with HA instead of GFP (data not shown). Thus, preventing for3p autoinhibition also bypasses the need for bud6p in NETO. In contrast, the *for3DAD** mutation did not restore bipolar growth in other NETO mutants, such as *tea1*Δ or *tea4*Δ, and it did not seem to cause premature bipolar growth in interphase wild-type cells (Figure 8D; data not shown). Thus, this effect of *for3DAD** was specific toward *bud6*Δ cells. In summary, all known phenotypes of *bud6*Δ cells—defective for3p localization, weak actin cables, and NETO failure—can be rescued by the *for3DAD** mutation. The simplest explanation for these effects is that bud6p has a primary role in relieving autoinhibition of for3p (see *Discussion*).

Bud6 Also Mediates Cortical Localization

Although bud6p was not required for for3pDAD* localization in the context of the whole protein, it was needed for the proper cell tip localization of for3C, the C-terminal fragment of for3p. Because this fragment cannot be autoinhibited, these effects of bud6p could not be explained solely by its effects on autoinhibition. Introduction of the DAD* mutation in for3C did not restore its localization to cell tips in *bud6*Δ cells, showing that the DAD* mutation itself did not somehow produce a novel cortical targeting signal (data not shown).

In *bud6* mutant cells, GFP-for3C failed to localize to cell tips, but it still decorated actin cables (Figure 7D). When we prevented actin cable association, either by LatA treatment or by using the FH2 I930A mutant, GFP-for3C in *bud6*Δ cells did not accumulate at cell tips, and it was instead completely diffuse (Figure 7D; data not shown). In contrast, GFP-for3N localized normally to both cell tips in *bud6*Δ cells. These results suggest that bud6p has two functions: one in regulating autoinhibition and the second as a physical tether that contributes toward its localization at cell tips. We note that this tethering function of bud6p is usually masked in the context of the full-length for3p protein because of a functionally redundant localization site in the N terminus.

Relationship of bud6p and cdc42p

Because bud6p and cdc42p seem to share functions in regulating for3p, we investigated the possible relationship between these proteins. Several lines of evidence suggest that these factors function in independent ways. First, cdc42p and bud6p bind different for3p domains. Second, cdc42p localized well to growing cell tips in *bud6*Δ cells (Figure 7E). Also, bud6p–GFP localization to cell tips was unaffected in *cdc42-1625* cells (Figure 7F). Third, *cdc42-1625* and *bud6*Δ mutants were synthetic lethal (at 25°C). Thus, cdc42p and bud6p may not act solely in a common pathway but rather

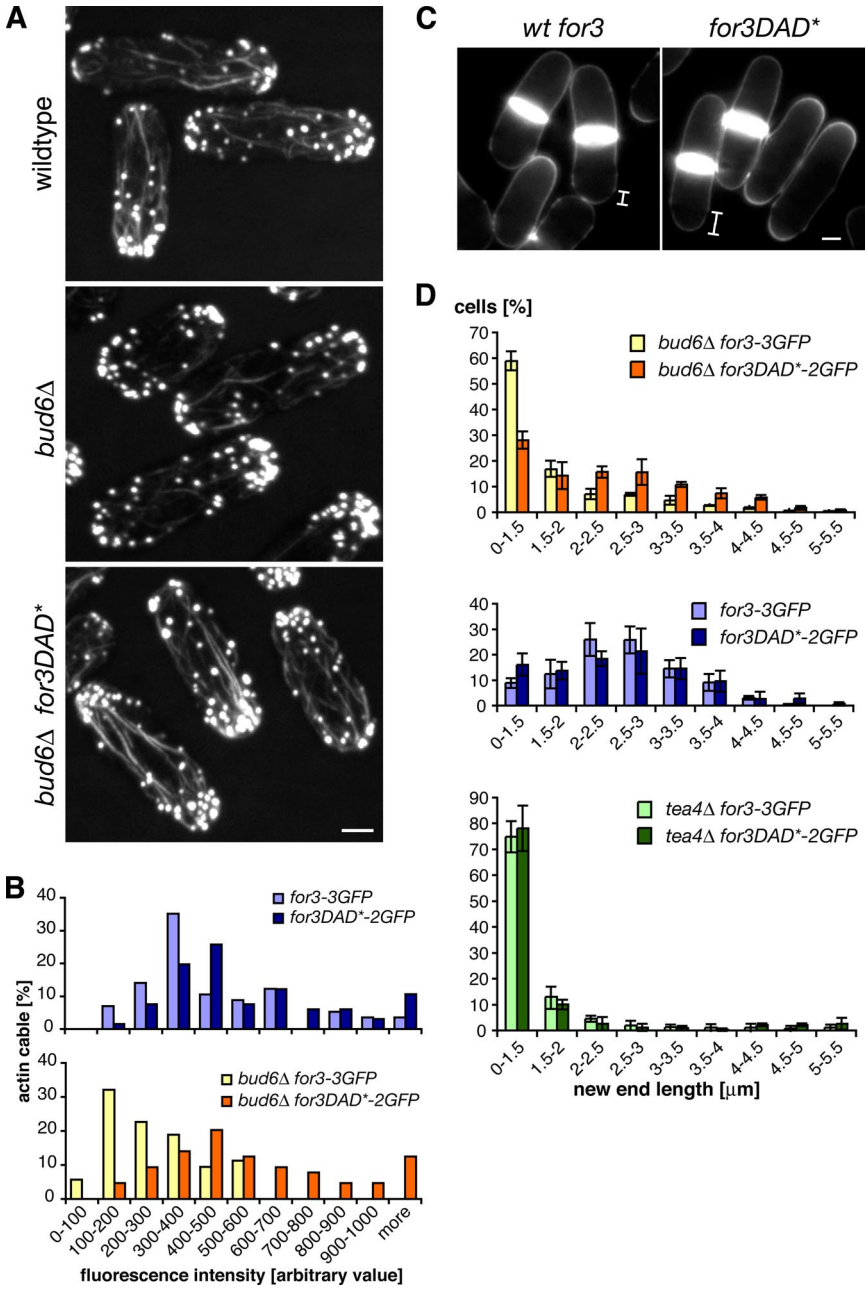

Figure 8. Mutation of the for3p DAD domain restores wild-type actin cables and bipolar growth in *bud6*Δ mutants. (A) Projection images of spinning disk confocal stacks of AlexaFluor 488-phalloidin–stained *for3-3GFP* (wild-type), *bud6*Δ *for3-3GFP* (*bud6*Δ), and *bud6*Δ *for3DAD*-2GFP* (*bud6*Δ *for3DAD**) cells. Note that the intensity of actin cables is lower in *bud6*Δ cells compared with wild-type cells, but that this phenotype is suppressed by the DAD* mutation. (B) Quantification of the fluorescence intensity of actin cables in *for3-3GFP*, *for3DAD*-2GFP*, *bud6*Δ *for3-3GFP*, and *bud6*Δ *for3DAD*-2GFP* cells, as in Figure 4E. (C) Calcofluor staining of *bud6*Δ cells expressing either *for3-3GFP* (wt *for3*) or *for3DAD*-2GFP* (*for3DAD**), showing monopolar and bipolar growth, respectively. (D) Quantification of new end growth in strains of the indicated phenotypes. The length between the inner side of the birth scar (black line in the calcofluor staining) and the tip of the cell was measured, as shown in C. This length is of up to 1.5 μm in cells that fail to initiate growth at the new end.

represent parallel pathways that both regulate for3p, as well as possibly other targets in cell polarization.

DISCUSSION

Here, we have dissected mechanisms of regulation and localization of the formin for3p. We show that for3p possesses at least two domains that mediate cell tip localization—in the N and C termini. A third domain, the FH2 domain, mediates its association with actin cables. Similar to diaphanous-related formins, the ability of for3p to localize and drive actin assembly depends on relieving the autoinhibitory binding of DAD and DID-like sequences at its N and C termini. Our results suggest that for3p in a closed, autoinhibited state cannot bind to cortical tethers and thus cannot localize. We provide evidence that for3p is converted to an open active conformation by cdc42p and bud6p. The active for3p can now bind to the cell tip and assemble actin filaments for construction of the actin cable.

Multiple Localization Domains Target for3p to Cell Tips

The anchoring of for3p at the cortex depends on at least two cortical tethers. Our data suggest that two sites on for3p mediate its localization to the cell tips, one site at the N terminus (in the vicinity of the DID domain) and one site near the C terminus. Bud6p, which binds in the vicinity of the DAD domain, is a likely cortical anchor for the C terminus. The corresponding cortical anchor(s) for the N terminus are not yet known. Tea4p is necessary for tethering for3N (as well as full-length for3p) at nongrowing cell ends, but because for3p still localizes to one cell tip in *tea4*Δ cells, additional factor(s) must contribute to tethering the formin to growing cell ends

(Martin *et al*., 2005). It is not clear yet whether cdc42p could be one such factor. Although for3pDAD* and a for3N fragment can still bind to cell tips in a *cdc42* mutant, this *cdc42* mutant does not represent a complete null.

For3p Autoinhibition

Like diaphanous-related formins, for3p is regulated by an intramolecular interaction between functional DAD and DID domains. The poor conservation of these domains with other formins raises the possibility that this mode of regulation may be more widely used even in "non-diaphanous-related" formins.

Our study of the *for3DAD** mutant revealed that autoinhibition has a surprisingly minor effect on the normal dynamic regulation of the formin. When the for3pDAD* mutant protein is expressed at endogenous levels, it has only mild effects on the organization of the actin cytoskeleton or cell growth, at least under the standard laboratory conditions tested. The amount of actin staining in each actin cable is increased, suggesting that there are more actin filaments within each bundle, or that individual filaments in the cable are longer. However, the rate of actin assembly, measured by the movement of for3p dots, was not increased, and the general organization of the actin cytoskeleton was normal. The DAD* did not obviously perturb the dynamic localization patterns of for3p, suggesting that this autoinhibitory regulation is not responsible for events such as its release from the cortex.

This mild phenotype is in contrast to studies in other cell types in which more dramatic effects are seen upon overexpression of truncated formin fragments (Watanabe *et al*., 1999; Tominaga *et al*., 2000; Evangelista *et al*., 2002; Sagot *et al*., 2002a; Dong *et al*., 2003; Koka *et al*., 2003; Schonichen *et al*., 2006). With these other studies, the more extreme effects may have been caused in part by formin overexpression and in part by the fact that formin fragments were likely delocalized from their intracellular location. It is possible that in fission yeast, most for3p molecules in the cell may normally already exist in the open conformation. In addition, for3p activity may be controlled by additional signals, such as through interactions with other proteins at the cell tips, or posttranslational modifications.

Cdc42p and Formin Regulation

Different Rho-formin pairs may regulate different actin structures in various cell types (Faix and Grosse, 2006). Our studies identify cdc42p as the yeast Rho family member needed for efficient actin cable assembly and for3p regulation in fission yeast. The five other Rho-GTPases have other functions in cell morphogenesis, and some are implicated in regulating cell wall synthesis; however, we note that our studies do not rule out minor or redundant contributions of these other Rhos on for3p regulation. Interestingly, none of them to date have been implicated in contractile ring assembly and cdc12p formin regulation in cytokinesis.

The suppression of *cdc42* by a *for3DAD** mutation provides strong evidence that cdc42p normally activates for3p by relieving its autoinhibition; in a *cdc42* mutant, for3p may be largely autoinhibited. These studies together with biochemical and structural data on many formins lead to a model in which cdc42p binding at the DID at the N terminus of for3p leads to relief of autoinhibition (Dong *et al*., 2003; Li and Higgs, 2003; Lammers *et al*., 2005; Otomo *et al*., 2005a; Rose *et al*., 2005; Nezami *et al*., 2006). However, because the *for3DAD** mutation does not suppress all of *cdc42* defects, it is likely that cdc42p has other effectors involved in cell polarization.

Bud6p and Multiple Aspects of Formin Regulation

Bud6p may regulate formin activity in multiple ways: through regulation of autoinhibition, as a cortical tether, and possibly as a cofactor in actin assembly. Our finding that the *for3DAD** mutant restores all the phenotypes ascribed to *bud6*Δ cells provides a strong genetic argument that bud6p functions primarily in vivo to antagonize autoinhibition. The binding of bud6p at a site at or near the DAD suggests an attractive model in which bud6p could block the DAD from binding to the DID. This is by far the simplest model to explain our data, and alternative models are considerably more complicated. For example, bud6p could activate for3p through some other mechanism, but the increase of activity of the for3pDAD* mutant may compensate for the decrease in activity in the *bud6*Δ mutant. However, this model would not account for how the *DAD** mutation restores for3p localization in *bud6*Δ cells. Future studies will be needed to test more directly the function of bud6p on autoinhibition.

Bud6p also seems to have a function as one of the cortical tethers that localize for3p at the cell tip. This function is redundant with tethers that bind around the DID domain. A third potential function is in regulation of actin assembly by the formin FH2 domain. In *S. cerevisiae*, in vitro experiments have shown that Bud6p binds to G-actin, accelerates nucleotide exchange on actin, and enhances the actin assembly activity of the Bni1p FH2 domain (Moseley *et al*., 2004). Bud6p thus may act like profilin to increase the local concentration of G-actin at the actin assembly site at the formin core. Because for3p activity has not been reconstituted in vitro yet, we have not been able to test the role of bud6p on this activity in the fission yeast proteins directly. However, the robust actin cables seen in a *bud6*Δ *for3DAD** mutant suggest that bud6p is not essential for the activity of a fully uninhibited formin in vivo.

The presence of multiple activating factors poses the question whether each modulates for3p independently, for example, in different cellular contexts, or whether they act in a concerted manner for full activation. For example, bud6p may prime the formin in a conformation to facilitate binding of cdc42p, or it may help to maintain for3p in the open conformation. Although obvious homologues of bud6p are not found outside of fungi, it will be interesting to investigate whether other formins are regulated at the C-terminal regions by analogous regulators. There is indeed some evidence from in vitro experiments that RhoA is not sufficient for full relief of mDia1 autoinhibition (Li and Higgs, 2003).

For3p and Regulation of Bipolar Growth

This work provides further evidence that the activation of for3p is a key step in establishment of bipolar growth at NETO. Two proteins required for NETO, tea4p and bud6p, have been identified to interact with and regulate for3p (Glynn *et al*., 2001; Feierbach *et al*., 2004; Martin *et al*., 2005). The ability of the *for3DAD** allele to restore NETO in *bud6* mutants suggests that the role of bud6p in NETO is to regulate for3p.

A current model for NETO is that, during polarity establishment in the G2 phase, for3p is recruited and activated at the new cell end by the concerted actions of at least three proteins: bud6p, cdc42p, and tea4p. Because expression of the *for3DAD** allele is not sufficient by itself for promoting bipolar growth in all cells, relief of autoinhibition is not the rate-limiting step in formin activation at NETO. However, relief of for3p autoinhibition by cdc42p and/or bud6p may be a necessary step to allow for3p to bind to cortical docking proteins present at the new end, such as tea4p. Bud6p,

which is also directly or indirectly recruited to the new end by tea1p and tea4p (Feierbach *et al*., 2004; Martin, unpublished observations), may also contribute to the tethering of for3p. At the new cell end, activation of actin assembly by the FH1–FH2 domains may be mediated by relief of autoinhibition and by other modes of activation, such as via tea4p (Martin *et al*., 2005). Localized formin-mediated assembly of actin cables then leads to initiation of polarized cell growth.

Other organisms may use similar autoinhibitory regulation of formins to modulate patterns of cell polarization: DAD-dependent regulation of a formin in *Ashbya gossypii* also affect the hyphal growth pattern of this filamentous fungus (Schmitz *et al*., 2006). Further investigation into these and other modes of formin regulation will reveal whether multiple activators also control formin autoinhibition in other species and provide a better understanding of the precise regulatory mechanisms underlying cell polarization and regulation of actin assembly.

ACKNOWLEDGMENTS

We thank Richard Benton and members of the Chang laboratory for critical reading of the manuscript and useful discussions. This work was supported by a Human Frontier Science Program Organization long-term fellowship (to S.G.M.), National Institutes of Health grant R01 GM-056836 (to F.C.), and grant BIO-2004-00384 from the Comisión Interministerial de Ciencia y Tecnologia (Spain) (to P.P.). S.A.R. was supported by a fellowship from the Spanish Ministerio de Educacion y Ciencia.

REFERENCES

Alberts, A. S. (2001). Identification of a carboxyl-terminal diaphanous-related formin homology protein autoregulatory domain. J. Biol. Chem. *276*, 2824–2830.

Cadwell, R. C., and Joyce, G. F. (1992). Randomization of genes by PCR mutagenesis. PCR Methods Appl. *2*, 28–33.

Chang, F., Drubin, D., and Nurse, P. (1997). cdc12p, a protein required for cytokinesis in fission yeast, is a component of the cell division ring and interacts with profilin. J. Cell Biol. *137*, 169–182.

Dong, Y., Pruyne, D., and Bretscher, A. (2003). Formin-dependent actin assembly is regulated by distinct modes of Rho signaling in yeast. J. Cell Biol. *161*, 1081–1092.

Eisenmann, K. M., Harris, E. S., Kitchen, S. M., Holman, H. A., Higgs, H. N., and Alberts, A. S. (2007). Dia-interacting protein modulates formin-mediated actin assembly at the cell cortex. Curr. Biol. *17*, 579–591.

Evangelista, M., Blundell, K., Longtine, M. S., Chow, C. J., Adames, N., Pringle, J. R., Peter, M., and Boone, C. (1997). Bni1p, a yeast formin linking cdc42p and the actin cytoskeleton during polarized morphogenesis. Science *276*, 118–122.

Evangelista, M., Pruyne, D., Amberg, D. C., Boone, C., and Bretscher, A. (2002). Formins direct Arp2/3-independent actin filament assembly to polarize cell growth in yeast. Nat. Cell Biol. *4*, 32–41.

Faix, J., and Grosse, R. (2006). Staying in shape with formins. Dev. Cell *10*, 693–706.

Feierbach, B., and Chang, F. (2001). Roles of the fission yeast formin for3p in cell polarity, actin cable formation and symmetric cell division. Curr. Biol. *11*, 1656–1665.

Feierbach, B., Verde, F., and Chang, F. (2004). Regulation of a formin complex by the microtubule plus end protein tea1p. J. Cell Biol. *165*, 697–707.

Gasman, S., Kalaidzidis, Y., and Zerial, M. (2003). RhoD regulates endosome dynamics through Diaphanous-related Formin and Src tyrosine kinase. Nat. Cell Biol. *5*, 195–204.

Gasteier, J. E., Madrid, R., Krautkramer, E., Schroder, S., Muranyi, W., Benichou, S., and Fackler, O. T. (2003). Activation of the Rac-binding partner FHOD1 induces actin stress fibers via a ROCK-dependent mechanism. J. Biol. Chem. *278*, 38902–38912.

Glynn, J. M., Lustig, R. J., Berlin, A., and Chang, F. (2001). Role of bud6p and tea1p in the interaction between actin and microtubules for the establishment of cell polarity in fission yeast. Curr. Biol. *11*, 836–845.

Hagan, I. M., and Hyams, J. S. (1988). The use of cell division cycle mutants to investigate the control of microtubule distribution in the fission yeast *Schizosaccharomyces pombe*. J. Cell Sci. *89*, 343–357.

Harris, E. S., Li, F., and Higgs, H. N. (2004). The mouse formin, FRLalpha, slows actin filament barbed end elongation, competes with capping protein, accelerates polymerization from monomers, and severs filaments. J. Biol. Chem. *279*, 20076–20087.

Harris, E. S., Rouiller, I., Hanein, D., and Higgs, H. N. (2006). Mechanistic differences in actin bundling activity of two mammalian formins, FRL1 and mDia2. J. Biol. Chem. *281*, 14383–14392.

Higgs, H. N., and Peterson, K. J. (2004). Phylogenetic analysis of the formin homology 2 (FH2) domain. Mol. Biol. Cell *16*, 1–13.

Johnson, D. I. (1999). Cdc *42*, An essential Rho-type GTPase controlling eukaryotic cell polarity. Microbiol. Mol. Biol. Rev. *63*, 54–105.

Kamasaki, T., Arai, R., Osumi, M., and Mabuchi, I. (2005). Directionality of F-actin cables changes during the fission yeast cell cycle. Nat. Cell Biol. *7*, 916–917.

Koka, S., Neudauer, C. L., Li, X., Lewis, R. E., McCarthy, J. B., and Westendorf, J. J. (2003). The formin-homology-domain-containing protein FHOD1 enhances cell migration. J. Cell Sci. *116*, 1745–1755.

Kovar, D. R., Harris, E. S., Mahaffy, R., Higgs, H. N., and Pollard, T. D. (2006). Control of the assembly of ATP- and ADP-actin by formins and profilin. Cell *124*, 423–435.

Kovar, D. R., Kuhn, J. R., Tichy, A. L., and Pollard, T. D. (2003). The fission yeast cytokinesis formin Cdc12p is a barbed end actin filament capping protein gated by profilin. J. Cell Biol. *161*, 875–887.

Kovar, D. R., and Pollard, T. D. (2004). Insertional assembly of actin filament barbed ends in association with formins produces piconewton forces. Proc. Natl. Acad. Sci. USA *101*, 14725–14730.

Lammers, M., Rose, R., Scrima, A., and Wittinghofer, A. (2005). The regulation of mDia1 by autoinhibition and its release by Rho*GTP. EMBO J. *24*, 4176–4187.

Li, F., and Higgs, H. N. (2003). The mouse Formin mDia1 is a potent actin nucleation factor regulated by autoinhibition. Curr. Biol. *13*, 1335–1340.

Li, F., and Higgs, H. N. (2004). Dissecting requirements for auto-inhibition of actin nucleation by the formin, mDia1. J. Biol. Chem. *280*, 6986–6992.

Martin, S. G., and Chang, F. (2005). New end take off: regulating cell polarity during the fission yeast cell cycle. Cell Cycle *4*, 1046–1049.

Martin, S. G., and Chang, F. (2006). Dynamics of the formin for3p in actin cable assembly. Curr. Biol. *16*, 1161–1170.

Martin, S. G., McDonald, W. H., Yates, J. R., 3rd, and Chang, F. (2005). Tea4p links microtubule plus ends with the formin for3p in the establishment of cell polarity. Dev. Cell *8*, 479–491.

Matheos, D., Metodiev, M., Muller, E., Stone, D., and Rose, M. D. (2004). Pheromone-induced polarization is dependent on the Fus3p MAPK acting through the formin Bni1p. J. Cell Biol. *165*, 99–109.

Michelot, A., Derivery, E., Paterski-Boujemaa, R., Guerin, C., Huang, S., Parcy, F., Staiger, C. J., and Blanchoin, L. (2006). A novel mechanism for the formation of actin-filament bundles by a nonprocessive formin. Curr. Biol. *16*, 1924–1930.

Miller, P. J., and Johnson, D. I. (1994). Cdc42p GTPase is involved in controlling polarized cell growth in *Schizosaccharomyces pombe*. Mol. Cell. Biol. *14*, 1075–1083.

Moseley, J. B., and Goode, B. L. (2005). Differential activities and regulation of *Saccharomyces cerevisiae* formin proteins Bni1 and Bnr1 by Bud6. J. Biol. Chem. *280*, 28023–28033.

Moseley, J. B., Sagot, I., Manning, A. L., Xu, Y., Eck, M. J., Pellman, D., and Goode, B. L. (2004). A conserved mechanism for Bni1- and mDia1-induced actin assembly and dual regulation of Bni1 by Bud6 and profilin. Mol. Biol. Cell *15*, 896–907.

Motegi, F., Arai, R., and Mabuchi, I. (2001). Identification of two type V myosins in fission yeast, one of which functions in polarized cell growth and moves rapidly in the cell. Mol. Biol. Cell *12*, 1367–1380.

Nakano, K., Imai, J., Arai, R., Toh, E. A., Matsui, Y., and Mabuchi, I. (2002). The small GTPase Rho3 and the diaphanous/formin For3 function in polarized cell growth in fission yeast. J. Cell Sci. *115*, 4629–4639.

Nezami, A. G., Poy, F., and Eck, M. J. (2006). Structure of the autoinhibitory switch in formin mDia1. Structure *14*, 257–263.

Otomo, T., Otomo, C., Tomchick, D. R., Machius, M., and Rosen, M. K. (2005a). Structural basis of Rho GTPase-mediated activation of the formin mDia1. Mol Cell *18*, 273–281.

Otomo, T., Tomchick, D. R., Otomo, C., Panchal, S. C., Machius, M., and Rosen, M. K. (2005b). Structural basis of actin filament nucleation and processive capping by a formin homology 2 domain. Nature *433*, 488–494.

Ozaki-Kuroda, K., Yamamoto, Y., Nohara, H., Kinoshita, M., Fujiwara, T., Irie, K., and Takai, Y. (2001). Dynamic localization and function of Bni1p at the sites of directed growth in *Saccharomyces cerevisiae*. Mol. Cell. Biol. *21*, 827–839.

Pelham, R. J., Jr., and Chang, F. (2001). Role of actin polymerization and actin cables in actin-patch movement in *Schizosaccharomyces pombe*. Nat. Cell Biol. *3*, 235–244.

Peng, J., Wallar, B. J., Flanders, A., Swiatek, P. J., and Alberts, A. S. (2003). Disruption of the diaphanous-related formin Drf1 gene encoding mDia1 reveals a role for Drf3 as an effector for Cdc42. Curr. Biol. *13*, 534–545.

Pring, M., Evangelista, M., Boone, C., Yang, C., and Zigmond, S. H. (2003). Mechanism of formin-induced nucleation of actin filaments. Biochemistry *42*, 486–496.

Pruyne, D., Evangelista, M., Yang, C., Bi, E., Zigmond, S., Bretscher, A., and Boone, C. (2002). Role of formins in actin assembly: nucleation and barbed-end association. Science *297*, 612–615.

Romero, S., Le Clainche, C., Didry, D., Egile, C., Pantaloni, D., and Carlier, M. F. (2004). Formin is a processive motor that requires profilin to accelerate actin assembly and associated ATP hydrolysis. Cell *119*, 419–429.

Rose, R., Weyand, M., Lammers, M., Ishizaki, T., Ahmadian, M. R., and Wittinghofer, A. (2005). Structural and mechanistic insights into the interaction between Rho and mammalian Dia. Nature *435*, 513–518.

Sagot, I., Klee, S. K., and Pellman, D. (2002a). Yeast formins regulate cell polarity by controlling the assembly of actin cables. Nat. Cell Biol. *4*, 42–50.

Sagot, I., Rodal, A. A., Moseley, J., Goode, B. L., and Pellman, D. (2002b). An actin nucleation mechanism mediated by Bni1 and profilin. Nat. Cell Biol. *4*, 626–631.

Schmitz, H. P., Kaufmann, A., Kohli, M., Laissue, P. P., and Philippsen, P. (2006). From function to shape: a novel role of a formin in morphogenesis of the fungus *Ashbya gossypii*. Mol. Biol. Cell *17*, 130–145.

Schonichen, A., Alexander, M., Gasteier, J. E., Cuesta, F. E., Fackler, O. T., and Geyer, M. (2006). Biochemical characterization of the diaphanous autoregulatory interaction in the formin homology protein FHOD1. J. Biol. Chem. *281*, 5084–5093.

Schott, D. H., Collins, R. N., and Bretscher, A. (2002). Secretory vesicle transport velocity in living cells depends on the myosin-V lever arm length. J. Cell Biol. *156*, 35–39.

Seth, A., Otomo, C., and Rosen, M. K. (2006). Autoinhibition regulates cellular localization and actin assembly activity of the diaphanous-related formins FRLalpha and mDia1. J. Cell Biol. *174*, 701–713.

Tominaga, T., Sahai, E., Chardin, P., McCormick, F., Courtneidge, S. A., and Alberts, A. S. (2000). Diaphanous-related formins bridge Rho GTPase and Src tyrosine kinase signaling. Mol Cell *5*, 13–25.

Verde, F., Mata, J., and Nurse, P. (1995). Fission yeast cell morphogenesis: identification of new genes and analysis of their role during the cell cycle. J. Cell Biol. *131*, 1529–1538.

Wallar, B. J., and Alberts, A. S. (2003). The formins: active scaffolds that remodel the cytoskeleton. Trends Cell Biol. *13*, 435–446.

Wallar, B. J., Stropich, B. N., Schoenherr, J. A., Holman, H. A., Kitchen, S. M., and Alberts, A. S. (2006). The basic region of the diaphanous-autoregulatory domain (DAD) is required for autoregulatory interactions with the diaphanous-related formin inhibitory domain. J. Biol. Chem. *281*, 4300–4307.

Watanabe, N., Kato, T., Fujita, A., Ishizaki, T., and Narumiya, S. (1999). Cooperation between mDia1 and ROCK in Rho-induced actin reorganization. Nat. Cell Biol. *1*, 136–143.

Watanabe, N., Madaule, P., Reid, T., Ishizaki, T., Watanabe, G., Kakizuka, A., Saito, Y., Nakao, K., Jockusch, B. M., and Narumiya, S. (1997). p140mDia, a mammalian homolog of Drosophila diaphanous, is a target protein for Rho small GTPase and is a ligand for profilin. EMBO J. *16*, 3044–3056.

Xu, Y., Moseley, J. B., Sagot, I., Poy, F., Pellman, D., Goode, B. L., and Eck, M. J. (2004). Crystal structures of a formin homology-2 domain reveal a tethered dimer architecture. Cell *116*, 711–723.